Handling Contacts in an Eulerian Frame A Finite Element Approach for Fluid-Structures with Contacts

Olivier Pironneau

To appear in the *International Journal of Computational Fluid Dynamics*
Vol. 32, No. 2-3, July 2018, 1–13

Handling Contacts in an Eulerian Frame
A Finite Element Approach for Fluid-Structures with Contacts

O. Pironneau *

*Paris-Sorbonne Université, LJLL-UPMC, Place Jussieu, Boite 187, F-75005

(*January 2018*)

Eulerian variational formulations for deformable solids, with or without fluids around them, end-up, after implicit time discretisation, as large non-linear systems for the velocities in the moving domains. Handling moving domains and moving boundaries requires careful meshing procedures; on the other hand the detection of contact is particularly simple with a distance function. Then at every time step a variational inequality can be used to update the velocities. This article gives new implementation details and two new complex simulations: a very soft bouncing ball in an axisymmetric flow and a disk hit by a club.

Keywords: Contact, Variational Inequality, Finite element Method, Eulerian Formulation.

Dedicated to Professor Mutsuto Kawahara

1. Introduction

With the sole knowledge of the boundaries, the detection of contact between two objects is not easy and requires appropriate data structures (see for example (S. Gottschalk, M. C. Liny and D. Manocha 1996)). For nonlinear elastic structures we are helped by the history of the shape deformations and handling contacts amounts to add a constraint to the minimisation of the potential energy of the problem (F. Schuricht 2002), and to solve a system of variational inequalities.

The Eulerian formulation of continuum mechanics is set in the physical moving domain and the unknown at each time step is the velocity field. Although there is no obvious added value compared to the Lagrangian formulation, contacts need no detection algorithm and are handled as if they always happen by adding an inequality constraints to the variational formulation.

For Fluid-Structure Interactions (FSI) the Eulerian formulation of nonlinear elasticity has been shown to be appropriate to fluid-structure interactions by Tomas Dune in his thesis (Th. Dunne and R. Rannacher 2006). Since then many authors have improved the method (see for example (Th. Richter and Th. Wick 2010)), including the present author (F. Hecht and O. Pironneau 2017).

One of the simplest contact problem is the rebound of a ball falling under its own weight in a fluid and bouncing on a flat hard surface. The Navier-Stokes equations for the fluid and nonlinear elasticity for the solid with matching velocities and constraints at the fluid-solid interfaces are sufficient and the ball will bounce due to the fluid force created by the thinning layer of fluid between the two surfaces; the phenomenon was reproduced numerically by (S. Frei 2016) but it requires a very fine mesh and tiny time steps.

Variational inequalities is an alternative to force admissible contacts into the equations of the problem. The method is well understood for contact with linear elasticity but still an open problem

*Corresponding author. Email: olivier.pironneau@gmail.com

for fluid-structure interactions (Baffico and T. Sassi 2015); yet we shall assume that variational inequalities describe correctly the physical problem of solid contact in a fluid.

In (F. Hecht and O. Pironneau 2017) a finite element method was shown to be energy stable for incompressible solids. The method and the energy estimates were generalised to Saint Venant-Kirchhoff materials in (O. Pironneau 2018); finally the 3D case was analysed in (Chen-Yu Chiang, O. Pironneau, Tony W. H. Sheu and M. Thiriet 2017). All these were done for fluid-structure systems. Generalisation to contacts was sketched only in (F. Hecht and O. Pironneau 2017); in this article we present the details of an implementation using a semi-smooth Newton algorithm and two new applications.

In paragraphs 2 and 3, the Eulerian method of (F. Hecht and O. Pironneau 2017) is recalled. Extension to contacts is described in paragraph 4, implementation details and numerical results in paragraph 5.

2. Eulerian Formulation of Non-Linear Elasticity

The laws of elasticity are usually written in a Lagrangian frame with $\mathbf{x}_0$ the spatial coordinate of a point particle at initial time and $\mathbf{X}(\mathbf{x}_0,t) := \mathbf{d}_0(\mathbf{x}_0,t)+\mathbf{x}_0$ its position at time t; $\mathbf{d}_0$ is the displacement field of the structure, so the structure is in the set $\Omega_s^t = \mathbf{X}(\Omega_0,t)$.

We use bold letters for vectors and tensors such as

$$\mathbf{X} = \begin{pmatrix} X_1 \\ X_2 \\ \dots \\ X_d \end{pmatrix}, \qquad \nabla\mathbf{X} = \begin{pmatrix} \partial_1 X_1 & \partial_1 X_2 & \dots & \partial_1 X_d \\ \partial_2 X_1 & \partial_2 X_2 & \dots & \partial_2 X_d \\ \dots & & & \\ \partial_d X_1 & & \dots & \partial_d X_d \end{pmatrix}$$

In an Eulerian framework the partial differential equations of elasticity are written in Ω_s^t and the displacement $\mathbf{d}$ is seen as a function of $\mathbf{x}\in\Omega_s^t$ and t. Since $\mathbf{x}_0 = \mathbf{X}^{-1}(\mathbf{x},t)$, we have that $\mathbf{d}(\mathbf{x},t) = \mathbf{d}_0(\mathbf{X}^{-1}(\mathbf{x},t),t)$.

2.1. *Incompressible Mooney-Rivlin Two Dimensional Structures*

The neo-Hookean Mooney-Rivlin incompressible law of elasticity is among the simplest; in 2 dimensions it has only one parameter c_1 and is given by the minimisation of the Kirchhoff potential (notice our notation for the matrix-product-trace ":" and ":=" for a definition):

$$\Psi = c_1\nabla\mathbf{X}:\nabla\mathbf{X} := c_1\mathrm{tr}(\nabla\mathbf{X}(\nabla\mathbf{X}))^T) = c_1\sum_{ij}(\partial_i\mathbf{X}_j)^2.$$

Then a fluid of density ρ_f and viscosity μ_f in interaction with such an elastic solid is given by the following system:

Find $\mathbf{u}, p, \Omega^t$ (velocity, pressure and domain), such that for all $\hat{\mathbf{u}}, \hat{p}$

$$\begin{cases} \displaystyle\int_{\Omega^t}[\rho \mathrm{D}_t\mathbf{u}\cdot\hat{\mathbf{u}} - p\nabla\cdot\hat{\mathbf{u}} - \hat{p}\nabla\cdot\mathbf{u}] + \int_{\Omega_f^t}\frac{\mu_f}{2}\mathrm{D}\mathbf{u}:\mathrm{D}\hat{\mathbf{u}} \\ \displaystyle + \int_{\Omega_s^t} c_1(\mathrm{D}\mathbf{d} - \nabla\mathbf{d}(\nabla\mathbf{d})^T):\mathrm{D}\hat{\mathbf{u}} = \int_{\Omega^t} f\hat{\mathbf{u}}, \\ \mathrm{D}_t\mathbf{d} := \partial_t\mathbf{d} + \mathbf{u}\cdot\nabla\mathbf{d} = \mathbf{u} \text{ in } \Omega_s^t. \end{cases} \tag{1}$$

where $\mathbf{f}$ is the field of volumic external forces, D is twice the symmetric gradient, ρ is the density, i.e. with $\mathbf{1}_\Omega(\mathbf{x}) = 1$ if $\mathbf{x} \in \Omega$, zero otherwise:

$$\mathrm{D}\mathbf{u} = \nabla\mathbf{u} + (\nabla\mathbf{u})^T, \quad \rho = \rho_s \mathbf{1}_{\Omega_s^t} + \rho_f \mathbf{1}_{\Omega_f^t}.$$

This systems contains the Navier-Stokes equations in the fluid region:

$$\rho_f(\partial_t\mathbf{u} + \mathbf{u}\cdot\nabla\mathbf{u}) - \mu_f(\nabla\mathbf{u} + \nabla\mathbf{u}^T) + \nabla p = \mathbf{f}, \quad \nabla\cdot\mathbf{u} = 0$$

Slip or no-slip or free-flow boundary conditions are imposed as usual by restricting the variational formulation. Notice that (1) contains also the equations for a fluid with a free surface.

Remark 1. *To prepare for the discretisation let us introduce a parameter δt and define $\bar{\mathbf{d}} = \mathbf{d} - \delta t\mathbf{u}$. Then, for a given $\bar{\mathbf{d}}$, evidently (1) is a variational problem for $\mathbf{u}, p$ in the fluid and the solid domain:*

$$\begin{cases} \displaystyle\int_{\Omega^t} [\rho \mathrm{D}_t\mathbf{u}\cdot\hat{\mathbf{u}} - p\nabla\cdot\hat{\mathbf{u}} - \hat{p}\nabla\cdot\mathbf{u}] + \int_{\Omega_f^t} \frac{\mu_f}{2}\mathrm{D}\mathbf{u} : \mathrm{D}\hat{\mathbf{u}} \\ \displaystyle + \int_{\Omega_s^t} \rho\delta t\Big[c_1(\mathrm{D}\mathbf{u} - \nabla\bar{\mathbf{d}}(\nabla\mathbf{u})^T - \nabla\mathbf{u}(\nabla\bar{\mathbf{d}})^T) : \mathrm{D}\hat{\mathbf{u}}\Big] \\ \displaystyle + \int_{\Omega_s^t} c_1(\mathrm{D}\bar{\mathbf{d}} - \nabla\bar{\mathbf{d}}(\nabla\bar{\mathbf{d}})^T) : \mathrm{D}\hat{\mathbf{u}} = \int_{\Omega^t} f\hat{\mathbf{u}}, \end{cases} \tag{2}$$

This formulation can be extended to Saint-Venant Kircchoff materials (see Appendix).

3. Time Discretisation

One of the key ingredient for accuracy and stability for Eulerian formulations is the discretisation of the convection operator D_t which appears twice in the variational formulation (1).

3.1. *Discretisation by the Characteristic-Galerkin Method*

Given a time step δt, denoting by $\mathbf{u}^n$ the value of $\mathbf{u}$ at $t = n\delta t$ and assuming smoothness, a Taylor expansion easily shows that if $\mathbf{a}$ is an incompressible velocity field,

$$(\partial_t\mathbf{u} + \mathbf{a}\cdot\nabla\mathbf{u})|_{x,(n+1)\delta t} = \frac{\mathbf{u}^{n+1} - \mathbf{u}^n o \mathrm{Y}}{\delta t}|_x + O(\delta t)$$

where $\mathrm{Y}(\mathbf{x})$ is any order-one approximation of $\mathcal{X}_{\mathbf{a}^m}(n\delta t)$, the solution at $\tau = n\delta t$ of

$$\frac{d\mathcal{X}}{d\tau}(\tau) = \mathbf{a}^m(\mathcal{X}(\tau)), \ \mathcal{X}((n+1)\delta t) = \mathbf{x}.$$

The simplest first order approximation is $\mathrm{Y}(\mathbf{x}) = \mathbf{x} - \mathbf{a}^m(\mathbf{x})\delta t$ with $m = n$ or $m = n+1$. (see (O. Pironneau and M. Tabata 2010) for details).

3.2. *A Fully Implicit Scheme*

With standard notations for the Sobolev spaces, in the case of Dirichlet boundary conditions on $\partial\Omega^n$, applying the Characteristic-Galerkin scheme leads to:

Find $\mathbf{u}^{n+1} \in \mathbf{H}_0^1(\Omega^{n+1}), p^{n+1} \in L_0^2(\Omega^{n+1})$, Ω_r^{n+1}, $r = s, f$, such that, with $\Omega^{n+1} = \Omega_f^{n+1} \cup \Omega_s^{n+1}$,

$\forall \hat{\mathbf{u}} \in \mathbf{H}^1_0(\Omega^{n+1})$, $\forall \hat{p} \in L^2_0(\Omega^{n+1}) := L^2(\Omega^{n+1})/\mathcal{R}$,

$$\int_{\Omega^{n+1}} \Big[\rho^{n+1}\frac{\mathbf{u}^{n+1}-\mathbf{u}^n\circ \mathrm{Y}^{n+1}}{\delta t}\cdot\hat{\mathbf{u}} - p^{n+1}\nabla\cdot\hat{\mathbf{u}} - \hat{p}\nabla\cdot\mathbf{u}^{n+1}\Big] + \int_{\Omega_f^{n+1}} \frac{\mu_f}{2}\mathrm{D}\mathbf{u}^{n+1} : \mathrm{D}\hat{\mathbf{u}}$$
$$+ \int_{\Omega_s^{n+1}} c_1\Big[\mathrm{D}(\mathbf{d}^n\circ\mathrm{Y}^{n+1}+\delta t\mathbf{u}^{n+1}) - \nabla(\mathbf{d}^n\circ\mathrm{Y}^{n+1}+\delta t\mathbf{u}^{n+1})(\nabla(\mathbf{d}^n\circ\mathrm{Y}^{n+1}+\delta t\mathbf{u}^{n+1})^T\Big] : \mathrm{D}\hat{\mathbf{u}} \tag{3}$$
$$= \int_{\Omega^{n+1}} \mathbf{f}\cdot\hat{\mathbf{u}}, \tag{4}$$
$$\Omega^{n+1} = (\mathrm{Y}^{n+1})^{-1}(\Omega^n) = \{\mathbf{x} :\ \mathrm{Y}^{n+1}(\mathbf{x}) := \mathbf{x} - \mathbf{u}^{n+1}(\mathbf{x})\delta t \in \Omega^n\} \tag{5}$$

Then update $\mathbf{d}$ by $\mathbf{d}^{n+1} = \mathbf{d}^n\circ\mathrm{Y}^{n+1} + \delta t\mathbf{u}^{n+1}$.

Discretisation in space by the finite element method is done as usual, by choosing compatible approximations for velocities and pressures leading to finite dimensional linear spaces $\mathbf{V}_{0h} \subset \mathbf{H}^1_0(\Omega^t)$ and $Q_h \subset L^2(\Omega^t)$. Because of the relation between $\mathbf{d}$ and $\mathbf{u}$ it is natural to take for $\mathbf{d}^n$ the same spatial approximation as that of $\mathbf{u}^n$. Except for interpolation errors to gris at different time times the discrete formulation is also unconditionally stable (see Theorem 1 below).

Consequently, a large non-linear system is to be solved at each time step. It can be solved by a fixed point algorithm on $\mathbf{u}^{n+1}, p^{n+1}$ with Ω^{n+1}, Y^{n+1} ρ^{n+1} temporarily frozen and a linearisation of the nonlinear term. Solve for $\mathbf{u}^{n+1}, p^{n+1}$:

$$\int_{\Omega} \Big[\rho\frac{\mathbf{u}^{n+1}-\mathbf{u}^n\circ \mathrm{Y}}{\delta t}\cdot\hat{\mathbf{u}} - p^{n+1}\nabla\cdot\hat{\mathbf{u}} - \hat{p}\nabla\cdot\mathbf{u}^{n+1}\Big] + \int_{\Omega_f} \frac{\mu_f}{2}\mathrm{D}\mathbf{u}^{n+1} : \mathrm{D}\hat{\mathbf{u}}$$
$$+ \int_{\Omega_s} c_1\Big[\mathrm{D}(\tilde{\mathbf{d}}+\delta t\mathbf{u}^{n+1}) - \nabla\tilde{\mathbf{d}}\nabla(\tilde{\mathbf{d}}+\delta t\mathbf{u}^{n+1})^T - \nabla(\delta t\mathbf{u}^{n+1})(\nabla\tilde{\mathbf{d}})^T\Big] : \mathrm{D}\hat{\mathbf{u}} = \int_{\Omega}\mathbf{f}\cdot\hat{\mathbf{u}}, \tag{6}$$

where $\tilde{\mathbf{d}} = \mathbf{d}\circ\mathrm{Y}$. Then these are updated at each fixed point iteration by their new values. Because of the energy estimates below it can be argued that the fixed-point method converges; our experience shows that 2 fixed point iterations are usually enough.

Remark 2. *Notice that (6) is a symmetric variational equation of the type:*

$$\mathbf{a}([\mathbf{u}^{n+1}, p^{n+1}], [\hat{\mathbf{u}}, \hat{p}]) = \mathcal{L}(\hat{\mathbf{u}}),\ \forall\hat{\mathbf{u}} \in \mathbf{H}^1_0(\Omega^{n+1}),\ \forall\hat{p} \in L^2_0(\Omega^{n+1}), \quad \textit{with} \tag{7}$$

$$\begin{aligned}\mathbf{a}([\mathbf{u},p],[\hat{\mathbf{u}},\hat{p}]) &:= \int_{\Omega}\Big[\rho\frac{\mathbf{u}}{\delta t}\cdot\hat{\mathbf{u}} - p\nabla\cdot\hat{\mathbf{u}} - \hat{p}\nabla\cdot\mathbf{u}\Big] + \int_{\Omega_f}\frac{\mu_f}{2}\mathrm{D}\mathbf{u} : \mathrm{D}\hat{\mathbf{u}}\\ &\quad + \int_{\Omega_s} c_1\delta t\Big[\mathrm{D}\mathbf{u} - \nabla\tilde{\mathbf{d}}(\nabla\mathbf{u})^T - \nabla\mathbf{u}(\nabla\tilde{\mathbf{d}})^T\Big] : \mathrm{D}\hat{\mathbf{u}}\\ \mathcal{L}(\hat{\mathbf{u}}) &:= \int_{\Omega}\rho\frac{\mathbf{u}^n\circ\mathrm{Y}}{\delta t}\cdot\hat{\mathbf{u}} - \int_{\Omega_s} c_1\Big[\mathrm{D}\tilde{\mathbf{d}} - \nabla\tilde{\mathbf{d}}\nabla\tilde{\mathbf{d}}\Big] : \mathrm{D}\hat{\mathbf{u}} + \int_{\Omega}\mathbf{f}\cdot\hat{\mathbf{u}},\end{aligned} \tag{8}$$

It could be solved by minimising $\frac{1}{2}\mathbf{a}([\mathbf{u},p],[\mathbf{u},p]) - \mathcal{L}(u)$ *in* $\mathbf{H}^1_0(\Omega)\times L^2_0(\Omega)$.

We recall the energy inequality obtained in (F. Hecht and O. Pironneau 2017) in terms of the Kirchhoff potential of the material Ψ.

Theorem 1.

$$\int_{\Omega^n}\frac{\rho^n}{2}|\mathbf{u}^n|^2 + \delta t\sum_{k=1}^{n}\int_{\Omega_f^k}\frac{\mu_f}{2}|\mathrm{D}\mathbf{u}^k|^2 + \int_{\Omega_s^0}\Psi^n \le \int_{\Omega_0}\frac{\rho^0}{2}|\mathbf{u}^0|^2 + \int_{\Omega_s^0}\Psi^0.$$

4. Formulation and Discretisation of Contact

4.1. *Rebound on a Flat Surface*

Let us begin with a simple case: the rebound of an elastic structure on a flat rigid plane of equation $x_2 = 0$.

At any time in the algorithm the updated structure must have: $\mathbf{x} \in \Omega_s^{n+1} \Rightarrow x_2 \geq 0$. This translates into: $x_2 + \delta t u_2^{n+1,k}(\mathbf{x}) \geq 0$ for all $\mathbf{x} \in \partial\Omega_s^{n,k}$. Here n is the time step and k is the fixed point iteration index to solve the nonlinear problem (3)-(5) by (7). Thus (7) must be replaced by

$$\min_{[\mathbf{u},p]\in\mathbf{H}^+}\{\frac{1}{2}\mathbf{a}([\mathbf{u},p],[\mathbf{u},p]) - \mathcal{L}(u)\} \text{ or } \min_{[\mathbf{u},p]}\max_{\lambda\leq 0}\{\frac{1}{2}\mathbf{a}([\mathbf{u},p],[\mathbf{u},p]) + \int_{\partial\Omega_s}\lambda(u_2 + \frac{x_2}{\delta t}) - \mathcal{L}(u)\}$$

where $\mathbf{H}^+ = \{\mathbf{H}_0^1(\Omega) \times L_0^2(\Omega) \ : \ x_2 + \delta t u_2(\mathbf{x}) \geq 0 \ \forall \mathbf{x} \in \partial\Omega\}$ and $\lambda \in L^2(\partial\Omega)$ is the Lagrange multiplier for the constraint.

Calculus of variations gives: find $\mathbf{u}, p, \lambda$ such that

$$\begin{aligned} &\lambda \leq 0, \quad u_2 + \frac{x_2}{\delta t}|_{\partial\Omega_s} \geq 0, \ \lambda(u_2 + \frac{x_2}{\delta t})|_{\partial\Omega_s} = 0 \\ &\mathbf{a}([\mathbf{u},p],[\hat{\mathbf{u}},\hat{p}]) + \int_{\partial\Omega_s\cap(\text{dist}<\epsilon)}\lambda\hat{u}_2 = \mathcal{L}(\hat{\mathbf{u}}), \quad \forall[\hat{\mathbf{u}},\hat{p}], \end{aligned} \tag{9}$$

where $\mathbf{x} \mapsto \text{dist}(\mathbf{x})$ is the distance of $\mathbf{x}$ to the plane $x_2 = 0$, i.e. x_2. This term has been added to reduce domain where contact is likely to occur, namely on the boundary and when two boundaries are close to each others.

Remark 3. *Exact contact poses a serious meshing problem; to avoid it we always use an approximate contact inequality with a tolerance (small) parameter tol, here:*

$$x_2 + \delta t u_2(\mathbf{x}) \geq tol$$

4.2. *Contact Between Two Moving Structures*

The above approach to contact can be generalised to 2 (or more) moving structures. Let the 2 boundaries nearing contact be indexed by $i = 1, 2$ and let $\mathbf{x}$ be on one of them, i.e. let $\mathbf{x} \in \partial^i\Omega_s^{n+1}$, be at a distance $\text{dist}^i(\mathbf{x})$ of $\Omega_s^{j\,n+1} \geq 0$, $j = 1, 2, \ j \neq i$.

Let $\mathbf{x}^*(\mathbf{x}) \in \Omega_s^{j\,n+1}$ be the point which realises $\text{dist}^i(\mathbf{x}) = |\mathbf{x} - \mathbf{x}^*(\mathbf{x})|$. An admissible displacement must be such that ($\mathbf{n}^k$ is the outer normal to the boundary of the k^{th} structure $\partial^k\Omega$) :

$$\mathbf{x}\cdot\mathbf{n}^k + \delta t\mathbf{u}(\mathbf{x})\cdot\mathbf{n}^k \leq \mathbf{x}^*(\mathbf{x})\cdot\mathbf{n}^k + \delta t\mathbf{u}(\mathbf{x}^*(\mathbf{x}))\cdot\mathbf{n}^k, \quad k = 1, 2$$

which is also $[\mathbf{u}(\mathbf{x}^*(\mathbf{x})) - \mathbf{u}(\mathbf{x})]\cdot\mathbf{n}^k \geq \text{dist}^i(\mathbf{x})/\delta t$.
So the variational equation to solve involves a Lagrange multiplier $\lambda \in L^2(\partial^1\Omega_s \cup \partial^2\Omega_s)$:

$$\mathbf{a}([\mathbf{u},p],[\hat{\mathbf{u}},\hat{p}]) - \int_{\partial\Omega_s\cap(\text{dist}<\epsilon)}\lambda\hat{\mathbf{u}}(\mathbf{x})\cdot\mathbf{n}(\mathbf{x}) = \mathcal{L}(\hat{\mathbf{u}})$$

Notice that the formulation is symmetric with respect to $\partial^1\Omega$ and $\partial^2\Omega$.

4.3. *The semi-smooth Newton method for the Rebound on a Flat Surface*

Such variational inequalities are easily solved by the semi-smooth Newton algorithm of (K. Ito and K. Kunisch 2003). First it is shown that for any $c \in \mathcal{R}^+$, (9) is equivalent to

$$\begin{cases} a([\mathbf{u},p],[\hat{\mathbf{u}},\hat{p}]) + <\lambda,\hat{\mathbf{u}}> = \mathcal{L}(\hat{\mathbf{u}}) \ \ \forall \hat{\mathbf{u}}, \quad \text{where } <\lambda,\mathbf{u}> := \displaystyle\int_{\partial\Omega_s \cap (\text{dist}<\epsilon)} \lambda u_2, \\ \lambda(\mathbf{x}) - \min\{0, \lambda(\mathbf{x}) + c\ (x_2 + u_2(\mathbf{x})\delta t)\} = 0 \ \ \forall \mathbf{x} \in \partial\Omega_s \cap (\text{dist}(\mathbf{x}) \leq \epsilon) \end{cases}$$

Note that this gives $\lambda(\mathbf{x}) \leq 0$ and $x_2 + u_2(\mathbf{x})\delta t \geq 0$. The semi-smooth Newton is an iterative loop:

4.3.0.1. Algorithm. Loop with $k = 0, 1...$,

Set	$I_k := \{\mathbf{x} \ : \ \lambda^k(\mathbf{x}) + c\ (x_2 + u_2^k(\mathbf{x})\delta t) < 0\}$
Solve for $\mathbf{u}^{k+1}$ the PDE	$\mathbf{a}([\mathbf{u}^{k+1}, p^{k+1}], [\hat{\mathbf{u}}, \hat{p}]) = \mathcal{L}(\hat{\mathbf{u}})$
with Dirichlet condition	$u_2^{k+1}(\mathbf{x}) = -x_2/\delta t, \ \forall \mathbf{x} \in I_k$
Solve for λ^{k+1} the variational form	$<\lambda^{k+1}, \hat{\mathbf{u}}> := \mathcal{L}(\hat{\mathbf{u}}) - \mathbf{a}(\mathbf{u}^{k+1}, \hat{\mathbf{u}}), \quad \forall \hat{\mathbf{u}}.$

Convergence is shown in (K. Ito and K. Kunisch 2003).

4.4. *The semi-smooth Newton method for the Bat Hitting a Disk*

At instant t^n, let $\mathbf{x}^1 \in \Gamma_1^n$ (e.g. bat), $\mathbf{x}^2 \in \Gamma_2^n$ (e.g. disk); the contact constraint is $dist(\mathbf{x}^j, \Gamma_k^n) > 0, \ j,k = 1,2, \ j \neq k$. Because all points in the solid regions are moved by $\mathbf{x} + \mathbf{u}^{n+1}(\mathbf{x})\delta t$, the constraint becomes

$$dist(\mathbf{x}^j + \mathbf{u}^{n+1}(\mathbf{x}^j)\delta t, \Gamma_k^{n+1}) > 0, \ j,k = 1,2, \ j \neq k$$

To estimate Γ_k^{n+1} we must find the point which realises the distance: $dist(\mathbf{x}^j, \mathbf{x}^{j*}) = dist(\mathbf{x}^j, \Gamma_k^n)$ and, for the bat-disk configuration, approximate the above by

$$\mathbf{n}(\mathbf{x}^j)\cdot(\mathbf{x}^{j*} + \mathbf{u}^{n+1}(\mathbf{x}^{j*})\delta t - (\mathbf{x}^j + \mathbf{u}^{n+1}(\mathbf{x}^j)\delta t)) = dist(\mathbf{x}^j, \Gamma_k^n) + \mathbf{n}(\mathbf{x}^j)\cdot\left(\mathbf{u}^{n+1}(\mathbf{x}^{j*}) - \mathbf{u}^{n+1}(\mathbf{x}^j)\right)\delta t > 0;$$

it is further approximated by

$$\delta t \mathbf{n}(\mathbf{x}^j) \cdot \left(\mathbf{u}^{n+1}(\mathbf{x}^j + 2d(\mathbf{x}^j)\mathbf{n}(\mathbf{x}^j)) - \mathbf{u}^{n+1}(\mathbf{x}^j)\right) + d(\mathbf{x}^j) > 0,$$

where $d(\mathbf{x}^j) = dist(\mathbf{x}^j, \Gamma_k^n)$.

For the bat-disk problem it is enough to write the above on the horizontal axis only:

$$u_1{}^{n+1}(\mathbf{x}) < u_1{}^{n+1}(\mathbf{x} + 2d(\mathbf{x})) + \frac{d(\mathbf{x})}{\delta t}, \quad \mathbf{x} \in \partial disk$$

Algorithm 4.3.0.1 holds but with $<\lambda,\mathbf{u}> := \displaystyle\int_{\partial disk} \lambda u_1$:

4.4.0.1. Algorithm. Loop with $k = 0, 1...$,

Set	$I_k = \{\mathbf{x} : \lambda^k(\mathbf{x}) + c({u_1}^{n+1}(\mathbf{x} + 2d(\mathbf{x})) + \dfrac{d(\mathbf{x})}{\delta t} - {u_1}^{n+1}(\mathbf{x}) < 0)$
Solve for $\mathbf{u}^{k+1}$ the PDE	$\mathbf{a}([\mathbf{u}^{k+1}, p^{k+1}], [\hat{\mathbf{u}}, \hat{p}]) = \mathcal{L}(\hat{\mathbf{u}})$
with Dirichlet condition	${u_1}^{k+1}(\mathbf{x}) = {u_1}^{n+1}(\mathbf{x} + 2d(\mathbf{x})) + \dfrac{d(\mathbf{x})}{\delta t}$
Solve for λ^{k+1} the variational form	$< \lambda^{k+1}, \hat{\mathbf{u}} >:= \mathcal{L}(\hat{\mathbf{u}}) - \mathbf{a}(\mathbf{u}^{k+1}, \hat{\mathbf{u}}),\ \forall \hat{\mathbf{u}}.$

A similar symmetric condition should be applied to the bat; but, on the ground that the bat is much harder than the disk, we haven't imposed any.

5. Implementation

The PDE solver FreeFem++ (F. Hecht 2012) has been used to program the method.

In the fluid, meshes are built with a Delaunay-Voronoi generator from the knowledge of boundaries and a parameter to control the density of vertices.

In the solid, discretized by a mesh with I vertices, $\{\mathbf{q}^i\}_{i=1}^I$, these are moved by their own velocities $\mathbf{u}(\mathbf{q}^i)$, i.e. ${\mathbf{q}^i}^{n+1} = {\mathbf{q}^i}^n + \mathbf{u}^{n+1}({\mathbf{q}^i}^n)$.

We have used linear finite elements for the pressure and quadratic element – on the same mesh– for the velocities and displacements.

Because meshes are different at each time step we need to project the velocity fields from the old mesh to the new mesh. This is done by a pointwise interpolation of degree 2. However, in the solid, an easier and more precise interpolation can be used because, when a quantity is convected by the same velocity field as the mesh motion, it has the same value at vertex ${\mathbf{q}^i}^n$ at time $n\delta t$ and at ${\mathbf{q}^i}^{n+1}$ at time $(n+1)\delta t$.

5.1. *Ball Bouncing on a Rigid plate in a Liquid*

An incompressible elastic ball in a tube filled with a Newtonian liquid falls by its own weight and rebounds on the bottom of the tube.

In order to treat this case we use an axisymmetric formulation in cylindrical coordinates. It can be checked that the Eulerian formulation of the problem for 3D axisymmetric geometries is also (1). To derive the equations in terms of radial and vertical coordinates r, z, we notice that the element of volume is $\mathrm{d}\mathbf{x} = r\mathrm{d}r\mathrm{d}z$, the differential operators are $\nabla \cdot \mathbf{u} = \partial_r u_r + \partial_z u_z + \dfrac{u_r}{r}$, and

$$\nabla\mathbf{u} = \begin{bmatrix} \partial_r u_r & 0 & \partial_r u_z \\ 0 & \dfrac{u_r}{r} & 0 \\ \partial_z u_r & 0 & \partial_z u_z \end{bmatrix}, \quad (\nabla\mathbf{u})^T = \begin{bmatrix} \partial_r u_r & 0 & \partial_z u_r \\ 0 & \dfrac{u_r}{r} & 0 \\ \partial_r u_z & 0 & \partial_z u_z \end{bmatrix}, \quad \mathrm{D}\mathbf{u} = \begin{bmatrix} 2\partial_r u_r & 0 & \partial_z u_r + \partial_r u_z \\ 0 & \dfrac{2u_r}{r} & 0 \\ \partial_z u_r + \partial_r u_z & 0 & 2\partial_z u_z \end{bmatrix}.$$

As the tensors appear only within the trace operator ":" in the variational formulation, the end product is no longer 3D. Finally as $\mathbf{u} = (u_r, 0, u_z)^T$,

$$\mathbf{u} \cdot \nabla\mathbf{d} = u_r\partial_r\mathbf{d} + u_z\partial_z\mathbf{d} = (u_r\partial_r d_r + u_z\partial_z d_r, 0, u_r\partial_r d_z + u_z\partial_z d_z)^T$$

The calculation rule then is to ignore the second component everywhere except in the tensors. This is an easy way to generate the equations in cylindrical coordinates.

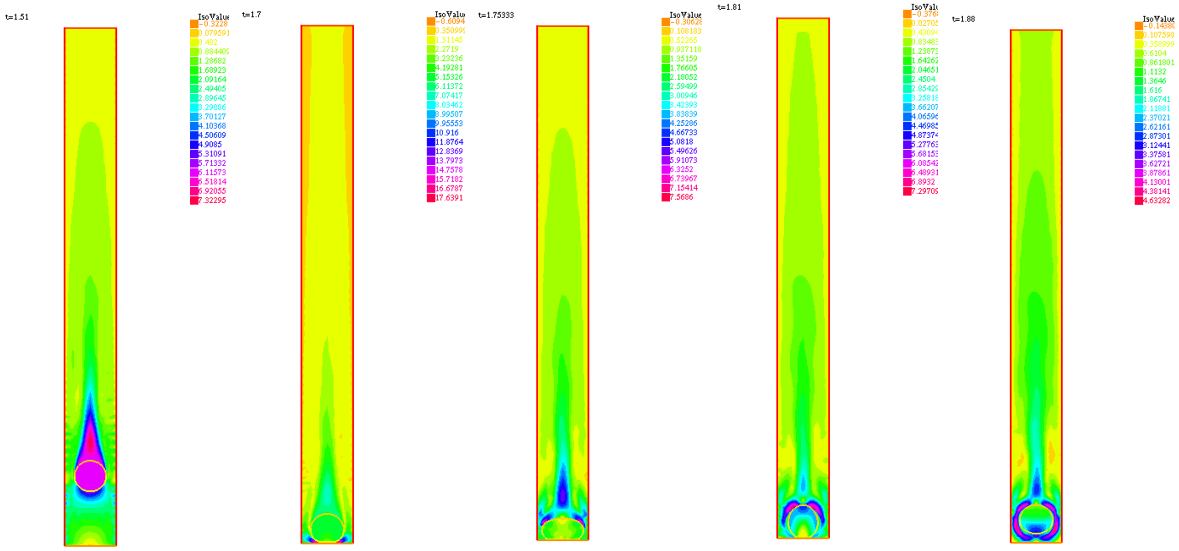

Figure 1. Color map of the norm of the velocity field at several instants of time (t=1.51, 1.7, 1.753, 1.81, 1.88) . Color maps are different for each snapshot; red indicates large values and yellow small ones.

5.1.1. Numerical Results

Consider a ball of radius $R = 0.3$, density $\rho_s = 5$, made of incompressible Mooney-Rivlin material (i.e. Poisson ratio =0.5) with $c_1 = \frac{1}{2}\mu_s = 100$, where the Lamé coefficients μ_s is related to the Young modulus by $E = 3\mu_s$.

The ball is released from rest near the surface (at height $H = 7$) in the center of a tube of height $L = 10$ and radius $R_t = 1$ filled with a liquid of density $\rho_f = 1$ and viscosity $\mu_f = 0.01$.

Sliding half a ball along the symmetry axis in cylindrical coordinates (r, z) poses remeshing problems. Instead we took a 2D geometry consisting of a cut of the 3D geometry along a radial plane and the numerical simulation is done in $[-R_t, R_t] \times [0, L]$. It is readily checked that cylindrical coordinates can be extended with $r < 0$.

When the ball is released it reaches a vertical velocity around -6 (fig 1) and then hit the bottom, deforms into an ellipsoid with flat bottom, and rebound by elasticity into an ellipsoid with longer vertical axis and then returns to the bottom, and so on several times.

To improve the precision near the rebound we made a simulation in a tube of height L=1.2 but with a ball with initial vertical velocity equal to -6 released at $H = 0.84$. Results are shown on figure 2 and on figure 3-right. On figure 3-left the position of the center of gravity is shown versus time. There, 8 smaller and smaller rebounds are clearly seen. One figure 3 -center the vertical diameter of the ball at its axis is shown versus time; this shows the rebounds and the oscillations from prolate to oblate ellipsoids between rebounds.

For all computations $T = 3$, $c = 100$, tol= 0.0166, $\rho_s = 5$, $\rho_f = 1$, $\mu_f = 0.01$. No slip conditions are applied to the fluid on the lateral and bottom surfaces of the tube. Computations are made with a "middle" mesh of 3011 vertices and $\delta t = 1/600$.

To see if the results are mesh dependent, figure 3-left draws the position of the center of gravity of the disk in 5 cases:

(1) a coarse mesh with 786 vertices and $\delta t = 1/400$,
(2) a middle mesh with 3011 vertices and $\delta t = 1/500$,
(3) a fine mesh with 6654 vertices and $\delta t = 1/600$,
(4) a very fine mesh with 11706 vertices and $\delta t = 1/700$.
(5) a middle mesh with 3011 vertices and $\delta t = 1/700$,

The results show a regular convergence with respect to the mesh size but the last case shows a

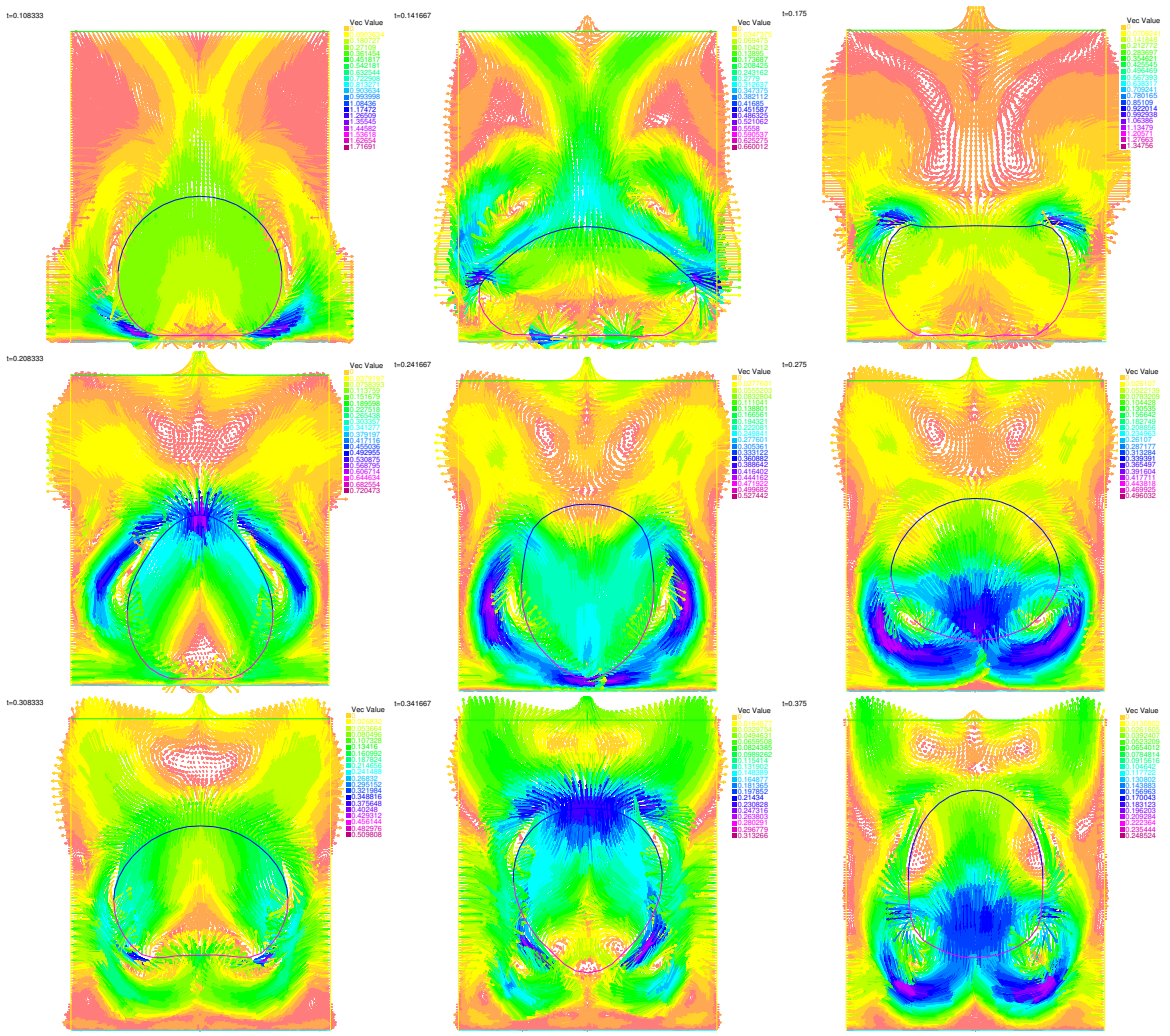

Figure 2. The velocity field at several instants of time (0.1083,0.1466,..), i.e. every 20 time steps. Colors are adjusted to the length of the velocity vectors. The computation is done in a short tube with slip velocities on the sides, no slip on the bottom and free flow on the top. The ball is released at time 0 with velocity -6. Color maps change for each snapshots.

stronger convergence on the time step size: the same precision is achieved with the middle mesh plus $\delta t = 1/700$ and the fine mesh plus $\delta t = 1/600$.

5.2. *Club Hitting a Disk in a Fluid*

A 2D club-like incompressible Mooney-Rivlin structure is at rest in a rectangular container $[0, 8] \times [0, 6]$ which is filled with a Newtonian incompressible fluid; the club's length is 4 and width 0.4 ; the rounded upper tip is clamped. A volumic force of intensity 5 is applied to it in the direction $\frac{5}{4}\pi$ during the whole session. An incompressible Mooney-Rivlin disk of radius 0.5 is also at rest in the rectangular container. Newman Boundary conditions are imposed on the boundary of the container except at the bottom where the velocity of the fluid is zero.

Due to the force, the club swings and hits the disk. The disk is pushed and acquires an horizontal velocity and leaves the club when the latter is called back due to its elastic structure. Hence this is a case of contact between two moving objects.

The parameters are shown on table 1. The constant c in the semi-smooth Newton algorithm is

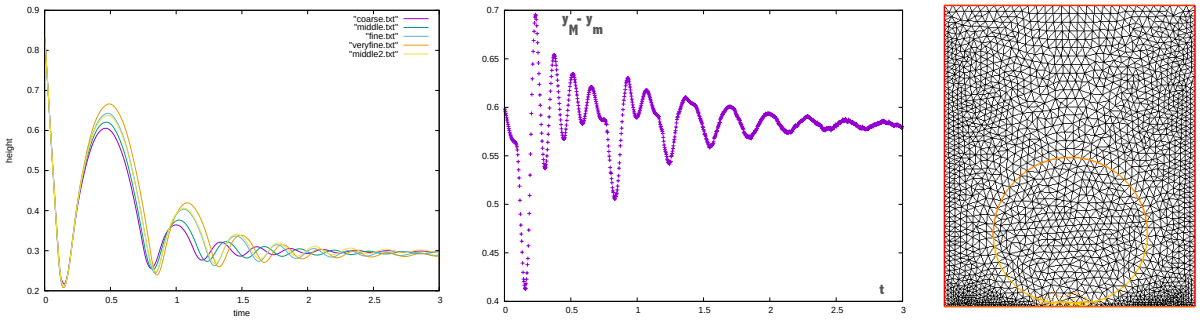

Figure 3. Left plot: position of the center of gravity of the ball versus time for 3 meshes, fine, middle and coarse, and two time steps for the middle mesh: 1/500 (middle) and 1/600 (middle2); this last case overlaps the fine mesh results. Center plot: vertical diameter of the ball versus time. Right plot: final position of the ball and middle mesh.

Table 1. The club-disk problem

	club	disk	fluid
density	50	500	0.01
c_1 or μ_f	10^5	$2 \cdot 10^4$	0.01
tol	0.1	0.1	

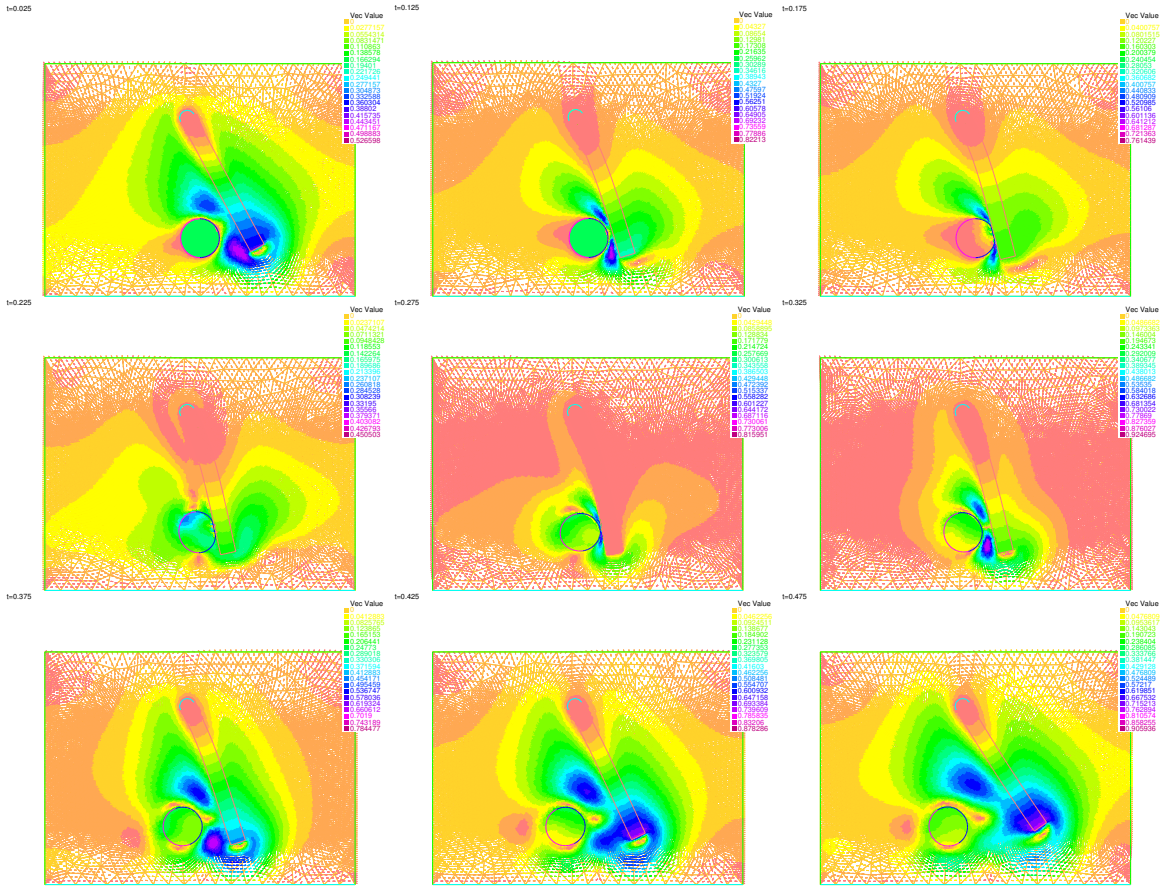

Figure 4. Club hiting a disk: the velocity field at several instants of time. The time of the snapshots are 0.025 and then 0.125, 0.175..., i.e. every twenty time steps.

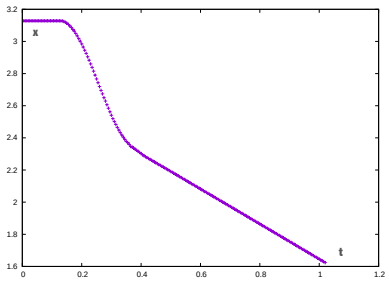

Figure 5. Club hitting a disk: the plot shows the horizontal position of the center of gravity of the disk versus time.

200. The time step is $T/2000$ with $T = 10$.

This last case is not robust. For several values of the parameters the FSI solvers blows-up, probably because the fixed point algorithm isn't robust enough; it may require a better nonlinear solver. But the contact algorithm does not appear to be the ingredient responsible for the blow-up; also the shock on the bat seems strong enough to induce vibrations which probably require an adapted time step or remeshing every now and then; a possible explanation for the blow-up which occurs usually much later after the contact. Let it be said also that the conservation of energy in the presence of contacts has not been established.

Instabilities have also been observed in the rebound of the ball due to the fact that we have chosen a very soft material and the fluid-structure interface develops kinks in certain circumstances. Such soft cases really need surface tension to be added.

References

Baffico and T. Sassi, Existence result for a fluid structure interaction problem with friction-type slip boundary condition. ZAMM Z. Angew. Math. Mech. 95, No. 8, 831-844,(2015).

Chen-Yu Chiang, O. Pironneau, Tony W. H. Sheu and M. Thiriet Numerical Study of a 3D Eulerian Monolithic Formulation for Incompressible Fluid-Structures Systems Fluids 2017, 2(2), 34; MDPI. Basel.

Th. Dunne and R. Rannacher Adaptive Finite Element Approximation of Fluid-Structure Interaction Based on an Eulerian Variational Formulation. In *Fluid-Structure Interaction: Modelling, Simulation, Optimization*. Lecture Notes in Computational Science and Engineering, vol 53. p110-146, H-J. Bungartz, M. Schaefer eds. Springer 2006.

S. Frei. Eulerian finite element methods for interface problems and fluid-structure interactions. Ph.D. dissertation, University of Heidelberg, 2016.

S Gottschalk, M C Liny and D Manocha. OBBTree A Hierarchical Structure for Rapid Interference Detection . ACM Siggraph Proceedings 1996.

F. Hecht New development in FreeFem++, J. Numer. Math., 20 (2012), pp. 251-265. www.FreeFem.org.

F. Hecht and O. Pironneau An Energy Stable Monolithic Eulerian Fluid-Structure Finite Element Method. IJNME, 2017.

K. Ito and K. Kunisch, Semi-Smooth Newton Method for Variational Inequalities of the First Kind, ESAIM:M2AN, Vol. 37, No 1, 2003, pp. 41–62.

O. Pironneau. An Eulerian Monolithic Fluid-Structure Formulation. *Anniversary volume in honor of P.G. Ciarlet. Li-Ta-Tsien ed. 2018. Also in hal.archives-ouvertes.fr/hal-01348648.*

O. Pironneau and M. Tabata. Stability and convergence of a Galerkin-characteristics finite element scheme of lumped mass type Int. J. Numer. Meth. Fluids 2010; 64:1240-1253.

Th. Richter and Th. Wick. Finite elements for fluid-structure interaction in ALE and fully Eulerian coordinates. Comput. Methods Appl. Mech. Engrg. 199 (2010) 2633-2642.

F. Schuricht, Calc Var (2002) 15: 433.

6. Appendix: Saint Venant-Kirchhoff Material

Similar monolithic formulations can be derived for compressible materials with a poly-convex Kirchhoff potential like hyper-elastic Saint-Venant-Kirchhoff materials with

$$\Psi = \frac{\lambda_s}{2}(\mathrm{tr}\mathbf{E})^2 + \mu_s \mathrm{tr}\mathbf{E}^2 \text{ with } \mathbf{E} = \frac{1}{2}(\nabla \mathbf{F}^T \nabla \mathbf{F} - \mathbf{I}).$$

The Eulerian formulation is (see O. Pironneau (2018)): find $\mathbf{u}, p, \Omega^t$ such that $\forall \hat{\mathbf{u}}, \hat{p}$,

$$\begin{cases} \displaystyle\int_{\Omega_f^t} \Big[\rho \mathrm{D}_t \mathbf{u} \cdot \hat{\mathbf{u}} - p\nabla\cdot\hat{\mathbf{u}} - \hat{p}\nabla\cdot\mathbf{u} + \frac{\mu_f}{2}\mathrm{D}\mathbf{u} : \mathrm{D}\hat{\mathbf{u}}\Big] \\ \displaystyle + \int_{\Omega_s^t} \rho\delta t\Big[b(\mathrm{D}\mathbf{u} - \nabla\bar{\mathbf{d}}(\nabla\mathbf{u})^T - \nabla\mathbf{u}(\nabla\bar{\mathbf{d}})^T) : \mathrm{D}\hat{\mathbf{u}} + \lambda_s \nabla\cdot\mathbf{u}\ \nabla\cdot\hat{\mathbf{u}}\Big] \\ \displaystyle + \int_{\Omega_s^t} \rho\Big[\mathrm{D}_t\mathbf{u}\cdot\hat{\mathbf{u}} + b(\mathrm{D}\bar{\mathbf{d}} - \nabla\bar{\mathbf{d}}(\nabla\bar{\mathbf{d}})) : \mathrm{D}\hat{\mathbf{u}} + (c + \lambda_s\nabla\cdot\bar{\mathbf{d}})\nabla\cdot\hat{\mathbf{u}}\Big] = \int_{\Omega^t} f\cdot\hat{\mathbf{u}} \\ \mathrm{D}_t\mathbf{d} = \mathbf{u},\ \bar{\mathbf{d}} = \mathbf{d} - \delta t\mathbf{u},\ \rho = \rho_s^0 \mathrm{det}_{\mathbf{I}-\nabla\mathbf{d}}\mathbf{1}_{\Omega_s^t} + \rho_f\mathbf{1}_{\Omega_f^t}, \end{cases} \tag{10}$$

with

$$\begin{aligned} &\gamma = (2 - 2\nabla\cdot\mathbf{d} + |\nabla\mathbf{d}|^2)J^2,\ \tilde{\gamma} = \gamma J^{-2} \\ &c = \lambda_s(\frac{1}{2}\gamma - 1)(\tilde{\gamma} - 1) + \mu_s(\gamma - J^2 - 1)\tilde{\gamma} - \lambda_s\nabla\cdot\mathbf{d}, \\ &b = \frac{1}{2}(\frac{\lambda_s}{2} + \mu_s)(\gamma - 1) - \frac{\lambda_s}{4} \end{aligned}$$

Here linear elasticity is visible because $b = \frac{\mu_s}{2} + O(u)$ and $c = O(u)$.

This section has been included for the reader to see that the method is not restricted to incompressible materials. Yet in this paper we report only on the incompressible case.

Acknowledgement

FreeFem is an open source high level user friendly software to solve PDEs by the finite element method. It runs on OSX, Windows, and Linux. It is downloadable from `www.freefem.org`. The FreeFem++ programs written for this article are available upon request to the author by email.